ISTITUTO NAZIONALE DI FISICA NUCLEARE
Laboratori Nazionali di Frascati

INFN-12-14/LNF
August 31, 2012

A possible hard X-ray FEL with the SuperB 6 GeV Electron Linac

D. Alesini[1)], M. P. Anania[1)], P. Antici[2)], D. Babusci[1)], A. Bacci[3)], A. Balerna[1)], R. Bartolini[4)], M. Bellaveglia[1)], M. Benfatto[1)], R. Boni[1)], R. Bonifacio[5)], M. Boscolo[1)], B. Buonomo[1)], M. Castellano[1)], L. Catani[6)], M. Cestelli-Guidi[1)], A. Cianchi[6)], R. Cimino[1)], E. Chiadroni[1)], S. Dabagov[1)], A. Gallo[1)], D. Di Gioacchino[1)], D. Di Giovenale[1)], G. Di Pirro[1)], A. Drago[1)], A. Esposito[1)], M. Ferrario[1)], F. Ferroni[2)], M. Gambaccini[7)], G. Gatti[1)], S. Guiducci[1)], R. Gunnella[8)], S. Ivashyn[9)], S. Lupi[2)], A. Marcelli[1)], M. Mattioli[2)], G. Mazzitelli[1)], A. Mostacci[2)], M. Migliorati[2)], E. Pace[1)], A. Perrone[10)], V. Petrillo[3)], R. Pompili[6)], C. Ronsivalle[1)], J. B. Rosenzweig[11)], A. R. Rossi[3)], W. Scandale[12)], L. Serafini[3)], O. Shekhovtsova[13)], B. Spataro[1)], C. Vaccarezza[1)], A. Vacchi[14)], A. Variola[12)], G. Venanzoni[1)], F. Villa[1)]

[1)] *INFN-Laboratori Nazionali di Frascati*
[2)] *INFN and Università "Sapienza" di Roma*
[3)] *INFN and Università di Milano*
[4)] *Diamond Light Source Ltd.*
[5)] *Universidade Federal da Paraiba, Brazil*
[6)] *INFN and Università di Roma "Tor Vergata"*
[7)] *INFN and Università di Ferrara*
[8)] *Università di Camerino*
[9)] *ITP, NSC - Kharkov Institute of Physics and Technology, Kharkov, Ukraine*
[10)] *INFN and Università del Salento*
[11)] *UCLA, Los Angeles, USA*
[12)] *LAL-Laboratoire de l'Accélérateur Linéaire, France*
[13)] *IFIC, Universitat de València-CSIC, Spain*
[14)] *INFN, Trieste*

Abstract

The possibility to drive a SASE X-ray FEL using the 6 GeV electron linac foreseen by the SuperB project has been recently considered. In this paper a preliminary design study based on FEL scaling laws supported by HOMDYN and GENESIS simulations is presented. The goal of this work is to provide a preliminary design study of the FEL system, based on state of the art normal conducting technology, suitable to conduct a realistic evaluation of the additional costs required to drive an FEL user facility making use of the SuperB linac.

Published by **SIDS-Pubblicazioni**
Laboratori Nazionali di Frascati

1. INTRODUCTION

After the successful demonstration of exponential gain in a Self Amplified Spontaneous Emission (SASE) Free Electron Laser (FEL) and the operation up to saturation at FLASH (5 nm) and LCLS (1 Angstrom), a number of short wavelength SASE-FEL projects have been funded or proposed world wide [1], oriented as user facilities. Free electron lasers are poised in fact to take center stage as the premier source of tunable, intense, monocromatic photons of either ultra-short time resolution or ultra-fine spectral resolution. The choice of FEL radiation wavelength ranges from infrared down to hard X-ray, and the adopted linac technology is based on normal conducting (S-band or C-band) or superconducting accelerating structures (L-band). In this context the possibility to drive a SASE X-ray FEL using the 6 GeV electron linac foreseen by the SuperB project [2] has been recently considered.

In this paper a preliminary design study based on FEL scaling laws [3] supported by HOMDYN [4] and GENESIS [5] simulations is presented. The goal of this work is to provide a preliminary design study of the FEL system, based on state of the art normal conducting technology, suitable to conduct a realistic evaluation of the additional costs required to drive an FEL user facility making use of the SuperB linac. Figure 1 shows a schematic layout of the SuperB linac system [2].

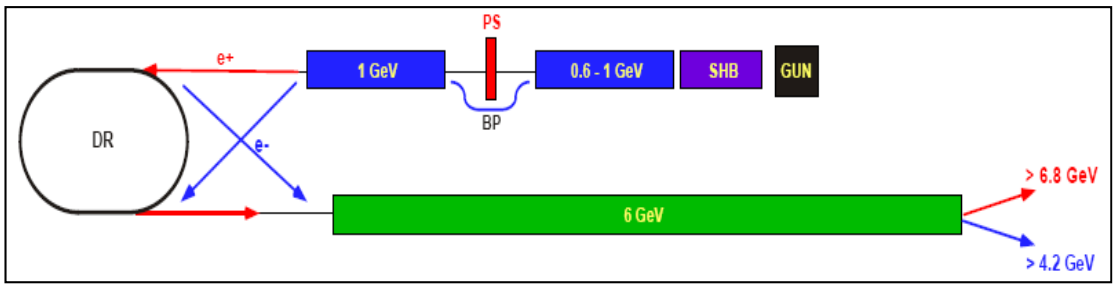

Figure 1 – SuperB injection system layout

As shown in the figure, electrons are accelerated up to 1-1.5 GeV in linac 1 and then injected into the damping ring (DR). The same electron beam, when impinging on a converter target, can be used to produce positrons. Linac 2 is used to capture and accelerate positrons up to 1 GeV before injection in DR. Both electron and positron beams are stored in DR for emittance damping. Linac 3 (green in the figure) provides additional 6 GeV to the beams in a 300 m long tunnel, with 87 S-band travelling wave accelerating structures operating at a maximum gradient of 23 MV/m, up to the required energy for injection in the SuperB main rings. Linac 3 can be conveniently used to drive also an FEL within the time sharing scheme discussed in the last section. Additional 150 m are available downstream linac 3 where the matching section, the undulators and the photon beam transport lines can be installed. Up to 60 m upstream linac 3 can be allocated for the FEL injection system.

2. FEL SCALING LAWS

When an electron beam traverses an undulator, it emits electromagnetic radiation at the resonant wavelength:

$$\lambda_r = \frac{\lambda_u}{2\gamma^2}\left(1 + a_u^2\right) \tag{1}$$

where λ_u is the undulator period, γ the beam relativistic factor and $a_u = K/\sqrt{2}$ for a planar undulator with undulator parameter given by $K = 0.934\lambda_u[cm]\hat{B}[T]$, being $\hat{B}$ the peak magnetic field. Figure 2 shows the achievable resonant wavelength versus λ_u and K, assuming a 6 GeV electron beam energy (γ = 11743). Using SPARC [6-9] like planar undulators with K = 2 and λ_u = 2.8 cm [10] one can expect an output radiation wavelength of 3 Angstrom. Shorter wavelength down to 1.8 Angstrom can be achieved by using an undulator with shorter period as the one foreseen for the future SPARC experiments with λ_u = 1.8 cm and K = 2.

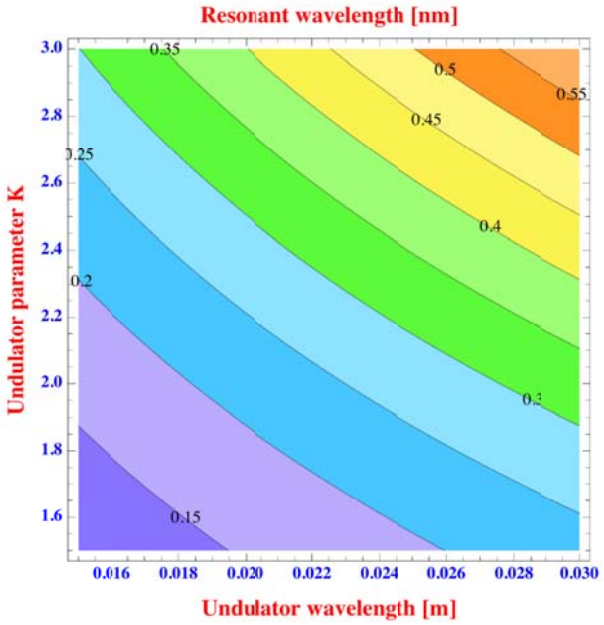

Figure 2 – Resonant wavelength λ_r versus undulator period λ_u and parameter K as predicted by eq. (1).

In a FEL billions of electrons cooperate to produce high peak power radiation within a narrow band around the resonant wavelength, provided that several conditions are satisfied, all depending on the FEL adimensional parameter ρ [11]:

$$\rho = \frac{1}{2\gamma}\left[\left(\frac{\hat{I}}{I_A}\right)\left(\frac{\lambda_u A_u}{2\pi\sqrt{\beta\varepsilon}}\right)^2\right]^{1/3} \tag{2}$$

where $\hat{I}$ is the electron beam peak current, I_A = 17 kA, β the betatron wavelength and $\varepsilon = \varepsilon_n/\gamma$ the geometrical emittance being ε_n the normalized emittance. For a planar undulator $A_u = a_u\left[J_o(\xi) - J_1(\xi)\right]$, where J are the Bessel functions and $\xi = a_u^2/2\left(1 + a_u^2\right)$.

In particular ρ represents the efficiency of system such that final saturation electromagnetic power emitted by an electron beam of power $P_b[TW] = E_b[GeV]\hat{I}[kA]$ is given by:

$$P_{sat} \approx \sqrt{2}\rho P_b \tag{3}$$

The undulator length required to achieve saturation, as predicted by the 3D model, is given by:

$$L_{sat}^{3D} \approx 20(1+\eta)L_G^{1D} \tag{4}$$

where

$$L_G^{1D} = \frac{\lambda_u}{4\sqrt{3}\pi\rho} \tag{5}$$

is the gain length predicted by the 1D model and $\eta = f(\eta_d, \eta_\varepsilon, \eta_\gamma)$ is a polynomial function of scaling parameters that accounts for the contribution of 3D effects: diffraction η_d, emittance η_ε and energy spread η_γ, as discussed in [3]. In our case the contribution of diffraction effects is dominant with respect to energy spread and emittance.

Equations (3) and (4) show that to maximize the extracted power within a minimum undulator length, one has to get the highest possible FEL parameter ρ. In addition optimal FEL performances in terms of minimal radiation bandwidth and transverse coherence can be achieved when the beam energy spread satisfies the following condition:

$$\frac{\sigma_\gamma}{\gamma} \le \rho \tag{6}$$

and the beam emittance is smaller of the radiation "emittance":

$$\varepsilon_n \le \gamma\lambda_r/4\pi \tag{7}$$

Equation (7) implies in our case that for a radiation wavelength of 3 Angstrom the normalized emittance has to be smaller than 0.3 μm. The difficulties to achieve such a high quality beam are partially mitigated by the fact that the radiation amplification process occurs on the scale of the cooperation length [12]:

$$L_{coop} = \frac{\lambda_r}{4\pi\rho} \tag{8}$$

over a *slice* of length $L_{slice} \approx 2\pi L_{coop}$ [12], typically much shorter than the bunch length, so that only bunch *slice* parameters are important for the FEL process, thus relaxing the conditions imposed by (6) and (7).

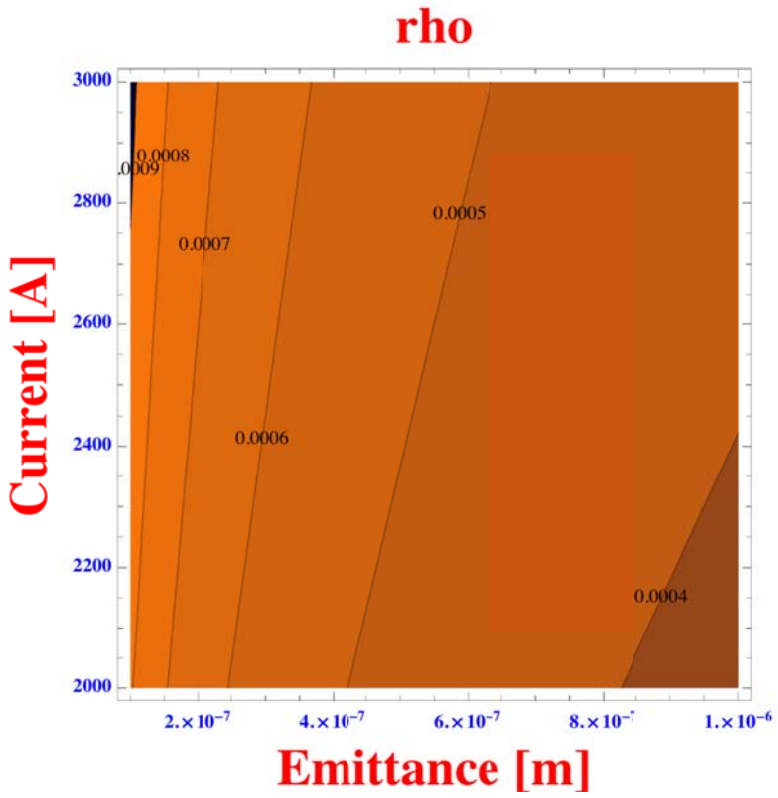

Figure 3 – ρ parameter versus emittance and peak current as predicted by eq. (2).

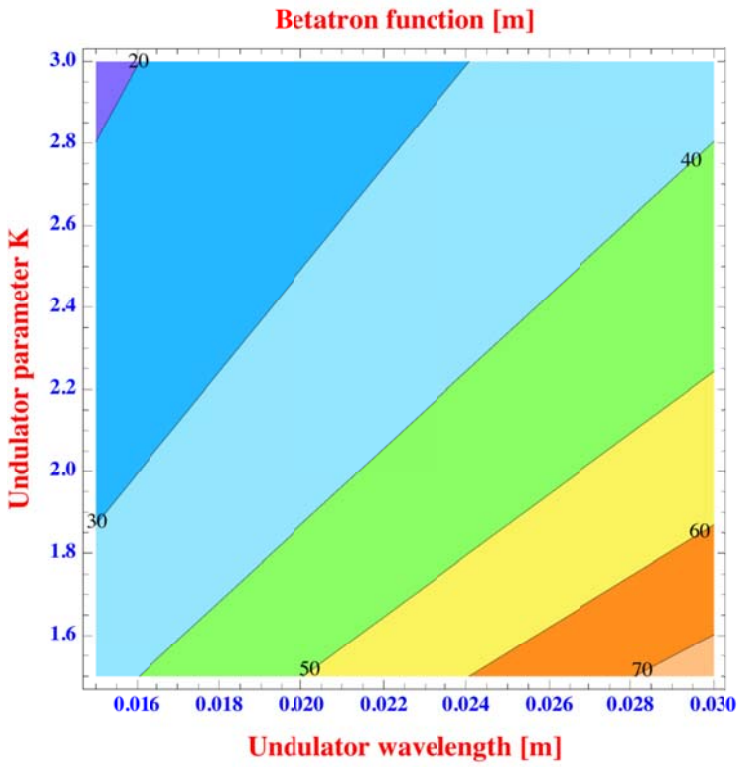

Figure 4- Betatron function versus undulator period λ_u and parameter K, as predicted by eq. (9).

Equation (2) shows that for a given undulator type, identified by its λ_u and K parameter, and a given electron beam energy γ, □□□□er ρ □can be obtained by increasing $\hat{I}$ and reducing ε_n. Figure 3 shows the dependence of the FEL parameter ρ on the beam quality in terms of peak current $\hat{I}$ and normalized emittance ε_n, assuming the beam is matched to the undulator natural focusing given by:

$$\beta = \frac{\gamma \lambda_u}{2\pi K} \tag{9}$$

shown also in figure 4.

With a peak current of 2.5 kA and a beam emittance of 0.5 μm the computed value of the FEL parameters results to be ρ = $5\text{x}10^{-4}$, giving a *slice* length of $L_{slice} = 0.4\mu m$ and a natural betatron function of 50 m (corresponding to a beam spot size σ_x = 47 μm), see also figure 4. Assuming a beam energy spread of 10^{-4}, thus satisfying condition (6), the corresponding extracted radiation power is about 10 GW with a saturation length of 60 m as shown in figure 5 and 6 respectively.

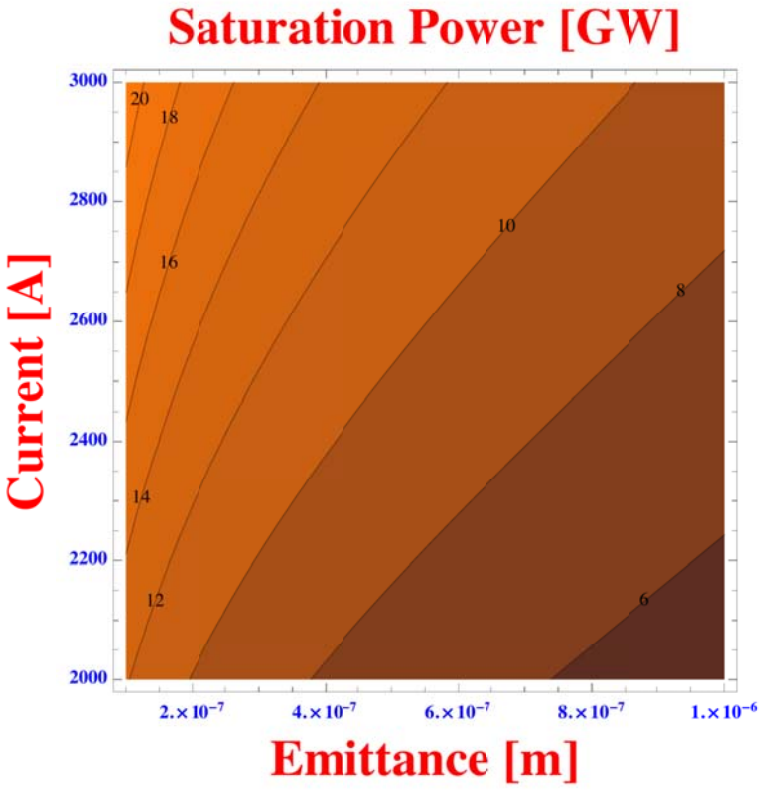

Figure 5 – Radiation power at saturation versus emittance and peak current, as predicted by eq. (3).

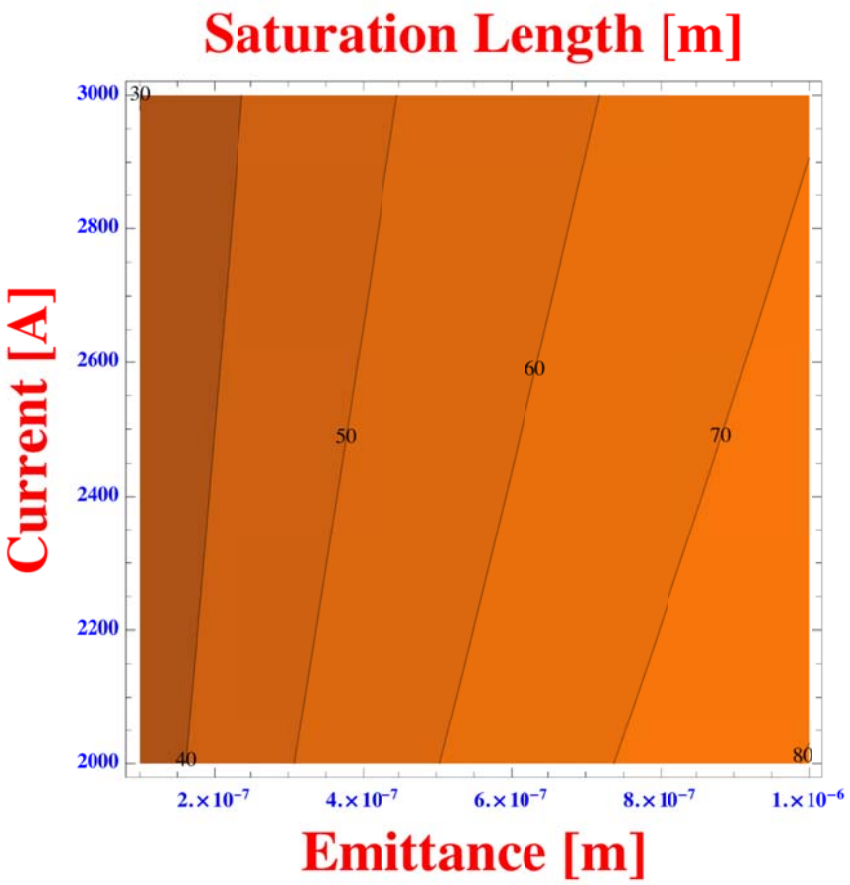

Figure 6 – Saturation length versus emittance and peak current as predicted by eq. (4).

This parametric study indicates to investigate the FEL performances and the driving beam parameters around the values reported in Table 1:

Table 1

E_b	λ_r	K	λ_u	I_{FWHM}	$\varepsilon_{n,rms}$	σ_γ/γ
6 GeV	3 A	2	2.8 cm	>2 kA	<1.5 μm	$<5\text{x}10^{-4}$

3. LINAC DESIGN STUDY

The optimization of a linac able to drive FEL experiments is quite a complicated task but the main requirement for the electron beam in order to achieve short wavelength radiation in a reasonable long undulator is clear: high transverse brightness. Transverse beam brightness is defined hereafter with the approximated expression:

$$B_\perp \approx \frac{2I}{\varepsilon_{n,x}\varepsilon_{n,y}} \tag{10}$$

where I is the bunch peak current and ε_n is the bunch transverse normalized emittance. The expected transverse brightness for electron beams driving short wavelength SASE FEL facilities is of the order of 10^{15} – 10^{16} A/m^2. Wake fields effects in accelerating sections and in magnetic bunch compressors contribute to emittance

degradation, hence the injector design and its operation is the leading edge for high quality beam production and for the success of the future light sources. RF guns, photo-cathode materials, laser pulse shaping and sub-ps synchronization systems are now a mature technology to produce high quality and stable beams [25]. In particular the technique termed "emittance compensation" [26] has been experimentally verified in many laboratories and theoretically well understood [27]. It is important to emphasize that high charge density beams experience two distinct regimes along the accelerator, depending on the laminarity parameter ρ_L defined as the ratio between the space charge and the thermal emittance ε_{th}:

$$\rho_L = \left(\frac{\hat{I}}{\gamma\gamma' I_A \varepsilon_{th}} \right)^2 \tag{11}$$

where I_A is the Alfven current, and $\gamma' \sim 2E_{acc}$ [MeV] is the normalised gradient. When $\rho >> 1$ the transverse beam dynamics is dominated by space charge effects. Correlated emittance oscillations are observed in this regime [28], caused by the different local current along the bunch and by finite bunch length effects. In this case mismatches between the space charge correlated forces and the external RF focusing gradient produce slice envelope oscillations that cause normalized emittance oscillations, also referred as plasma oscillations.

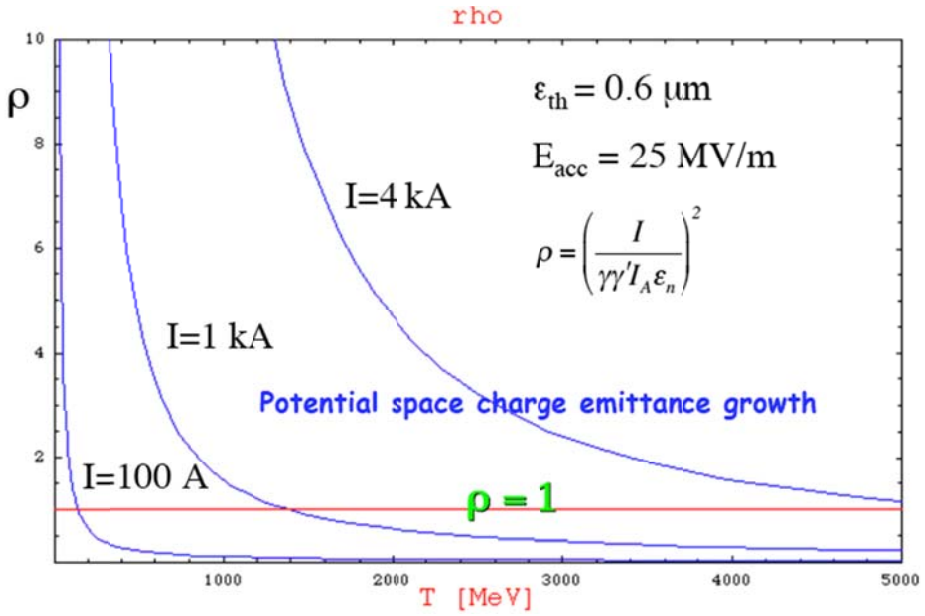

Figure 7: Laminarity parameter ρ versus beam energy T for different beam currents. Notice for example that a 1 kA beam is space charge dominated up to ~1 GeV.

It has been shown that to conveniently damp emittance oscillations the beam has to be injected into the booster with a laminar envelope waist ($\sigma' = 0$) and the booster accelerating gradient has to be properly matched to the beam size σ, energy γ and peak current $\hat{I}$, according to the following condition [27]:

$$\gamma' = \frac{2}{\sigma} \sqrt{\frac{\hat{I}}{2 I_A \gamma}} \tag{12}$$

By accelerating the beam, a transition occurs to the so-called emittance dominated regime, when $\rho << 1$, in this case the transverse beam dynamics is dominated by the emittance and correlated effects are not anymore observed. In case of bunch compressor systems are foreseen along the linac space charge effects might become important again and the transition from space charge to emittance dominated regime shift at higher energy, see Fig. 7. In this case the whole linac behaves like a long injector [20] and the same matching condition (12) should be applied also at higher energy.

In this section we illustrate a possible layout of the electron linac able to produce the required high brightness beam to drive the X-ray FEL discussed in the previous section. We decided in this study to minimize the impact on the SuperB linac design, including only the indispensable hardware modifications needed to achieve the expected beam parameters reported in table 1. We decided also to consider only single bunch operation at moderated charge per bunch (200 pC) with a repetition rate of 33 Hz, fully compatible with the operation of the SuperB linac with the SLED option.

The beam dynamics study of the photo-injector and linac described here has been performed with the HOMDYN [4] code. HOMDYN is a fast running code whose main approximation consists in supposing the bunch as a uniformly charged cylinder divided in *slices*. The evolution of each *slice*, longitudinally and transversally, is described by envelope equation where electromagnetic fields are assumed to be linear. Moreover transverse and longitudinal wake fields are included [13]. On the other hand Coherent Synchrotron Radiation and related micro-bunching effects in the magnetic compressor are not yet included.

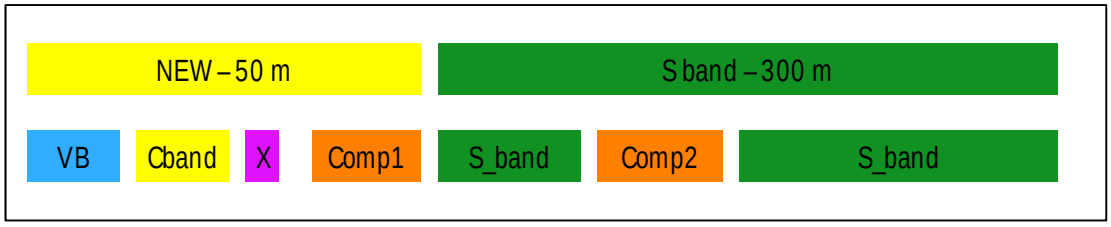

Figure 8 – Upper plot: shematic layout of the SuperB linac (green) and the new XFEL injection system (yellow). Lower plot: details of the foreseen modifications.

Figure 8 shows a schematic layout of the XFEL linac: in the upper plot is shown the SuperB main linac in green, hosted in the 300 m long tunnel, and the new FEL injection system in yellow, located in the 50+10 m long Damping Ring bunker. The lower plot details the foreseen modifications. Notice that a 30 m long magnetic compressor system (Comp2) has to be included in a bypass line of the main linac, thus reducing the available accelerating sections for the XFEL beam (the SuperB beam won't be affected making use for example of pulse dipole magnets). It follows that the FEL injection system has to provide also the missing energy to achieve the final 6 GeV.

We have investigated the following layout for the FEL injection system:

- *S-band injection system* (2856 MHz) composed by one 1.6 cell RF photoinjector followed by 2 TW structures embedded in a solenoid magnetic field as required to operate in the Velocity Bunching mode. A copy of the existing SPARC_LAB photoinjector. 8 m long.

- *C-band linac* (5712 MHz) with 13 TW structures operating 15 degrees off crest to drive the downstream first magnetic compressor. A similar design is foreseen for the ELI_NP linac project. 27 m long.
- *2 X-band structures* (11.424 GHz). 1.5 m long. The beam loses here about 100 MeV.
- *Magnetic Compressor 1* for the first bunch length compression stage to increase the peak current at least up to 720 A in a 8 m long magnetic chicane with R_{56} = 23 mm.

The S-band injector operates at 125 MV/m in the RF gun and at 25 MV/m in the accelerating structures, driving the beam to an energy of 75 MeV in the compression mode. The bunch is compressed with the velocity bunching technique [14,15] reaching a peak current of 145 A, corresponding to a compression ratio of a factor 4.4 The beam is then injected in the downstream C-band linac [16] operating at an accelerating field of 35 MV/m to boost the beam up to 750 MeV, driving the beam out of the space charge dominated regime. The beam is accelerated along the C-band linac 15 degrees out of crest to fulfill the downstream magnetic compressor requirements: the induced energy spread is 0.4% thus allowing a magnetic chicane (with R_{56}=23 mm) to compress the beam to 25 μm length with a final current of 720 A, a gentle compression ratio of a factor 5. Two X band accelerating structures [17] operating at 60 MV/m field in the decelerating phase reduce the longitudinal beam emittance as required by the downstream compressor systems. In this configuration the whole linac is 45 m long.
The beam parameters at the exit of the FEL injection system are reported in Table 2.

Table 2

E_b	I_{FWHM}	$\varepsilon_{n,rms}$	σ_γ/γ
600 MeV	720 A	1 μm	4×10^{-3}

The FEL beam is then injected in the SuperB S-band linac including the following subsystems:

- *S-band linac 3a* to boost the beam up to 2.3 GeV with 25 TW structures operating at an accelerating field of 23 MV/m, 20 degrees off crest to drive the downstream second magnetic compressor.
- *Magnetic Compressor 2* for the second bunch length compression stage to increase the peak current up to 2 kA in a 30 m long magnetic chicane with R_{56} = 18 mm.
- *S-band linac 3b* to boost the beam up to the final energy of 6 GeV with 54 TW structures operating at an accelerating field of 23 MV/m, on crest to damp the beam energy spread with contribution of the longitudinal wake field effects.

The beam parameters at the exit of the FEL injection system are reported in Table 3.

Table 3

E_b	I_{FWHM}	$\varepsilon_{n,rms}$	σ_γ/γ	σ
6 GeV	2 kA	1.2 μm	4.2×10^{-4}	10 μm

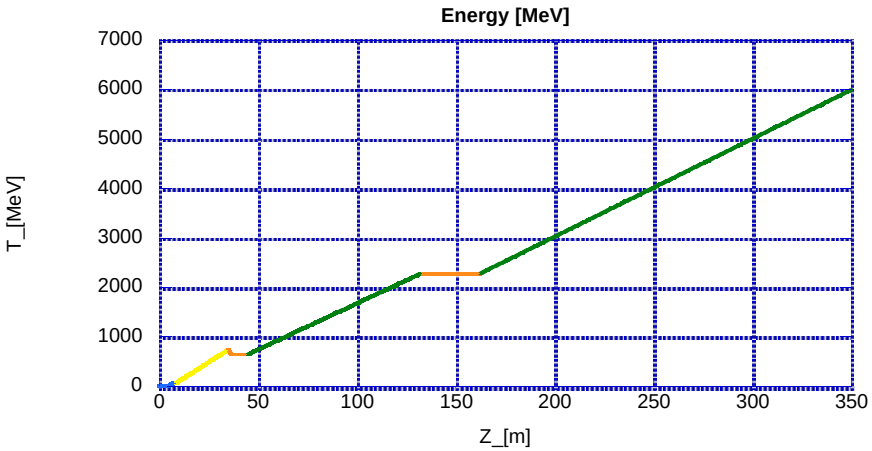

Figure 9 – Beam energy gain evolution along the linac.

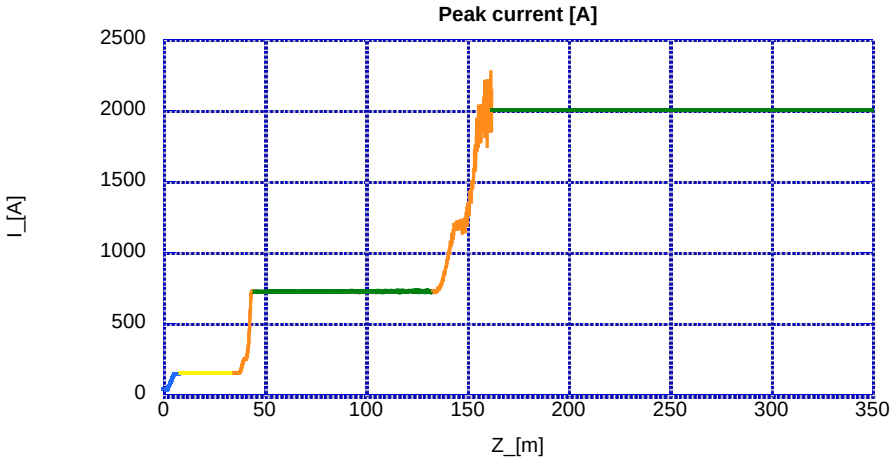

Figure 10 – Beam peak current evolution along the linac.

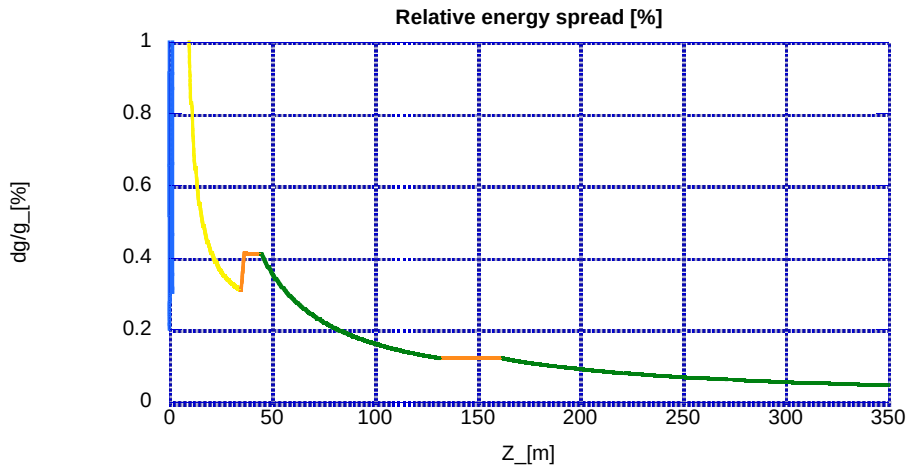

Figure 11 – Beam energy spread evolution along the linac.

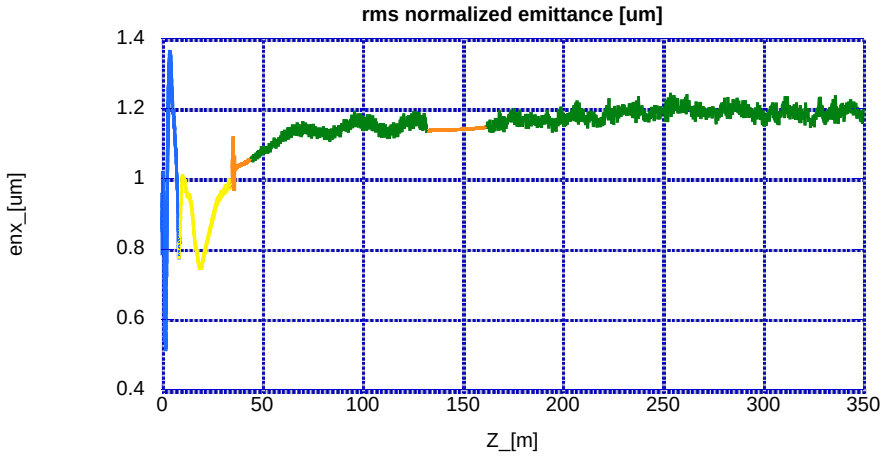

Figure 12 – Beam rms normalized emittance evolution along the linac.

Figures 9,10,11 and 12 illustrate the evolution along the full linac of the beam energy, peak current, energy spread and normalized emittance. The line colors are consistent with the schematic layout of Figure 8.

This preliminary investigation show that the parameters listed in Table 1 are reachable with the proposed layout with expected *slice* parameters even better than the one of Table 3, resulting in a beam brightness $B_{\perp} > 10^{15}$ A/m^2. Some concern about the compressor systems arising from the oversimplified model adopted in HOMDYN should be clarified by using more advanced code like PARMELA [18] and ELEGANT [19]. In addition the transition from the C-band linac to the S-band linac has to be matched with a more careful analysis. For example the transfer line from the C-band linac to the S-band linac can be used by itself as a compressor. Notice that in this study we have transported the beam matched to the RF focusing only, as it is possible in a high brightness electron beam [20]. More standard focusing by means of quadrupoles should be also investigated in order to keep under control possible quadrupole components of the RF fields. The matching section with the undulator at 6 GeV has not been investigated.

4. FREE ELECTRON LASER SIMULATIONS

Two basic single-pass SASE XFEL options have been investigated with simulations made with the GENESIS 1.3 code [5] and are presented in this section. The assumed electron beam *slice* parameters at the undulator entrance, consistent with the results reported in Table 3, are shown in Table 4.

Table 4

E_b	I_{slice}	$\varepsilon_{n,slice}$	σ_γ/γ
6 GeV	2.5 kA	0.6 μm	1 x10^{-4}

The current is supposed to have a Gaussian profile with a peak value I_{peak}=2.5 kA and a rms width σ_z=10 μm. Emittances of 0.6 μm in both planes and an energy spread *slice* value of 10^{-4} have been assumed. Two different cases have been investigated:

- SPARC-like undulators [10], with period λ_u =2.8 cm,
- shorter period undulator with λ_u =1.8 cm

with both undulators parameters summarized in Table 5.

Table 5

	SPARC-like	Short period
Period λ_u (cm)	2.8	1.8
a_{w0} (=K/$\sqrt{2}$)	1.51	1.2
Section length (m)	3.36	2.16
Gap length (m)	0.42	0.27
λ_r(Å)	3.16	1.525
σ_x(μm)	66	50
σ_y(μm)	40	35
β(m)	50	32

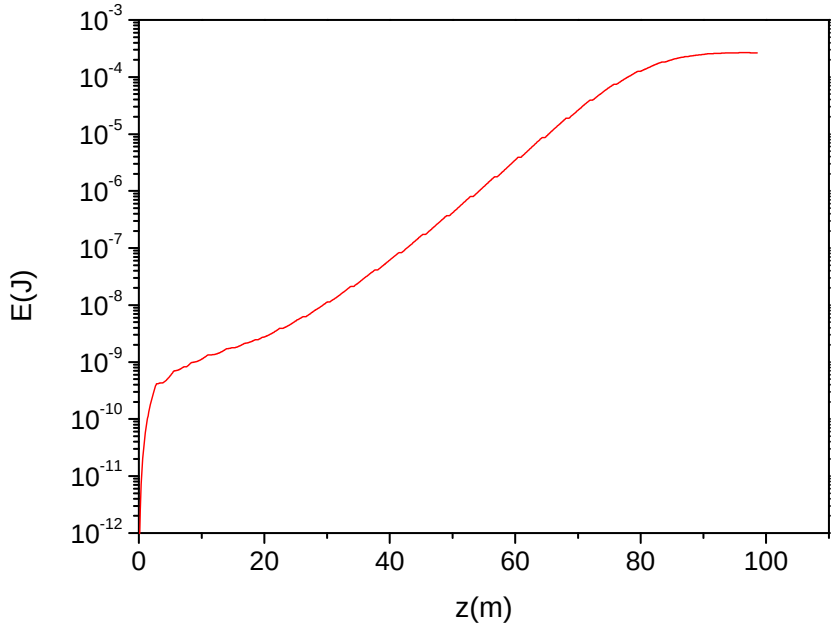

Figure 13 – Energy [J] vs coordinate z [m] along the undulator chain for the SPARC-like case.

In the first case the achievable wavelength is λ_r = 3.16 Angstrom. Optimum matching conditions have been considered. The radiation growth is shown in Figure 13 , and the radiation power and spectrum at the end of the undulator in Figure 14 and 15. The onset of saturation is at ~80-90 m *including gaps between undulator modules* (~11 m), and the total energy extracted is 270 μJ . The gain length estimated from figure 13 is slightly less than 5 m. In Table 6 (second column) the radiation parameters for this case are summarized. The far field at the end of the undulator is characterized by the presence of one single transverse mode.

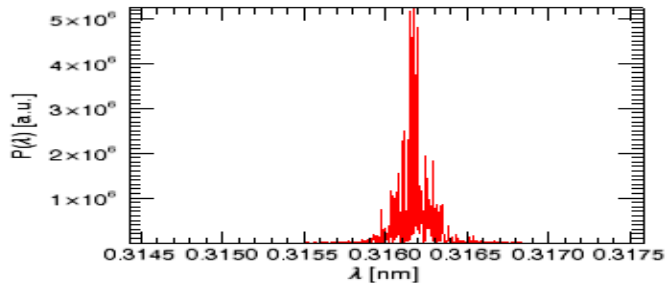

Figure 14 – Radiation spectrum at the end of the undulator chain, SPARC-like case

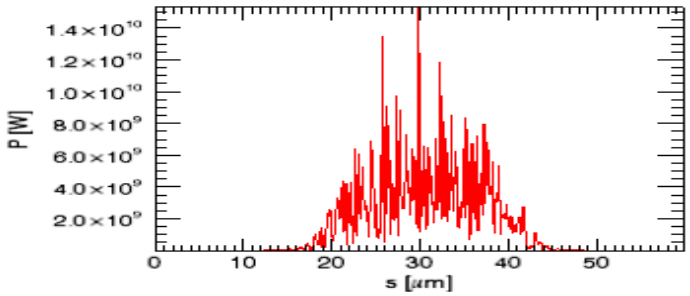

Figure 15 – Radiation power density at the end of the undulator chain, SPARC-like case.

Table 6

	SPARC-like	Short period
λ_r(Å)	3.16	1.525
L_s(m)	~90	~78
E_s(μJ)	270	114
bw(%)	0.04	0.023
L_g(m)	~4.8	~4.4

The second case analyzed is a short period undulator, whose characteristics are summarized in Table 5 (second column). The radiation parameters are reported in Table 6 (third column). In this case the resulting wavelength is λ_r =1.525 Angstrom. The radiation goes to saturation in about 80 m at an energy level of 114 μJ. Energy growth, spectrum and power distribution at the end of the undulator are respectively in figures 16,17 and 18.

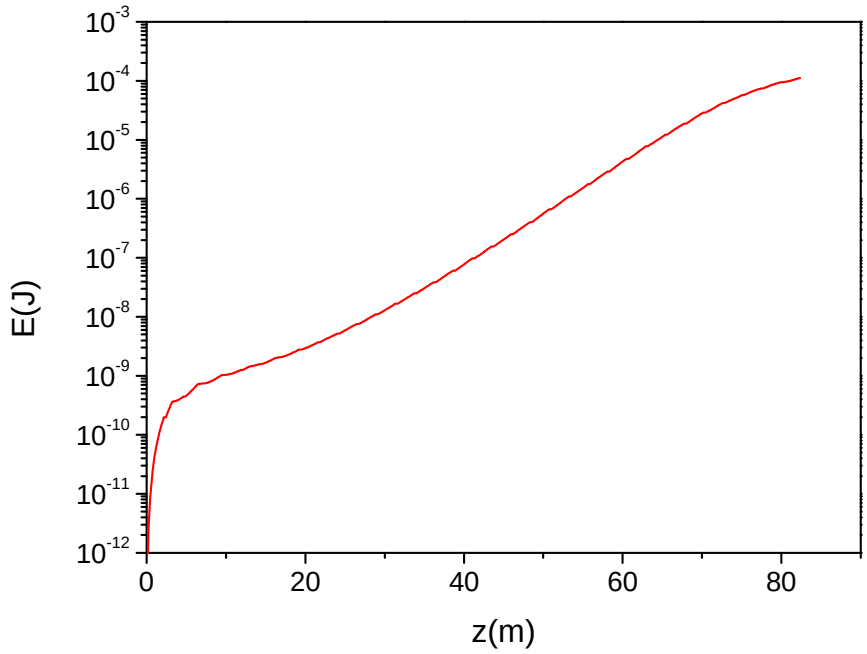

Figure 16 - Energy(J) vs coordinate z(m) along the undulator for the short period case

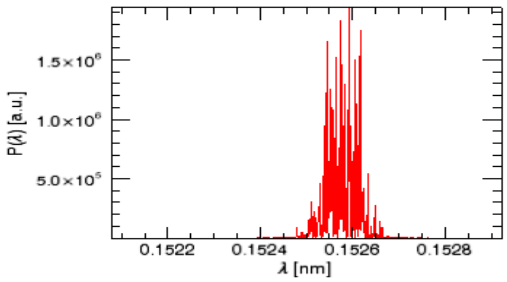

Figure 17 - Radiation spectrum at the end of the undulator chain, short period case.

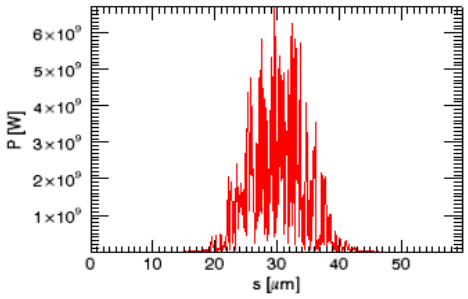

Figure 18 – Radiation power density at the end of the undulator chain, short period case.

An increase of the radiation yield could be obtained in both cases by improving the characteristics of the beam, or by increasing the current.

5. TIME SHARING BETWEEN XFEL AND SUPERB OPERATION

The time sharing between the 3 different beams, e+ ed e- for SuperB injection, and e- for XFEL is described below and schematically represented in Figure 19.

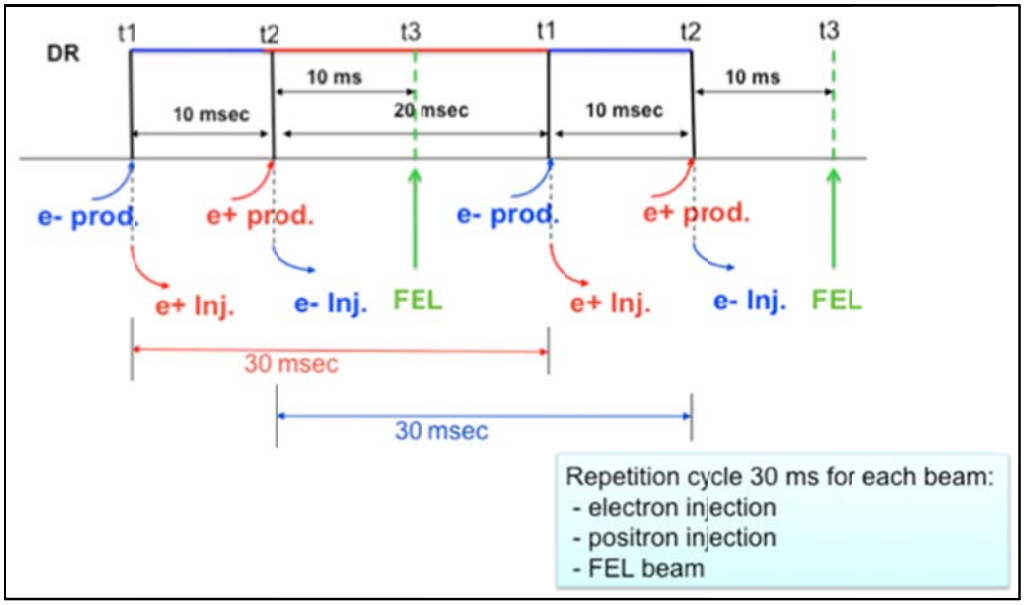

Figure 19 - Shared time between XFEL and SuperB injection

In order to achieve the emittance required for HER injection, positrons need to be stored in the DR for ~3 damping times, i.e. for 20 ms. Since the electrons have a lower initial emittance they can get the required emittance for LER injection with a store time of 10 ms. If the linac repetition frequency is 100 Hz it is possible to accelerate in the linac a pulse for the XFEL during the store time of the positrons in the DR without affecting the injection rate for SuperB. As it is shown in Figure 19 it is possible to provide a repetition cycle of 30 ms for each beam: positron injection, electron injection and a dedicated linac pulse for XFEL. The time duration available for the XFEL pulse, due to the SLED system used for the linac cavities, is of the order of 100 ns. This scheme is different from that described in the "SuperB Progress Report" [2] where the linac repetition frequency is 50 Hz, both the electron and positron beams are stored in the damping ring for 20 ms and the injection repetition cycle is 50 ms for each beam. The increase of the linac repetition frequency up to 100 Hz allows to use the linac to accelerate an electron beam pulse for an XFEL in time sharing with SuperB injection and to increase the repetition rate for the positron injection, which is the most demanding.

6. CONCLUSIONS

A preliminary design study of a possible X-ray FEL source making use of the SuperB electron linac has been presented in this paper. A large number of improvements are still possible for the linac design, giving a better beam quality in terms of emittance and peak current, able to produce a higher photon flux with a shorter saturation length. Some critical aspect should be also solved, as the need of a laser heater, the best position of the X-band cavities, the transfer lines and the compressor systems, the matching of the beam with the focusing channel according to condition (12). A more systematic study on these issues is under way.

More advanced FEL scheme than SASE should be also considered to improve the radiation quality (coherence), for example: "Self-seeding" [29], "High-gain harmonic generation", "Seeded harmonic cascade" or the possibility to produce ultra-short pulses at the atto-second level. To extend the user opportunity, the electron beam could be also extracted at a lower energy (~3 GeV) and used to produce radiation in the soft X-ray range with a reach user program, as in the case of the the SPARX project [22].

Furthermore a role of great relevance will be played by the development of dedicated X ray detectors. The signal to noise characteristics of the Silicon Drift Detectors (SDD) of large area developed by INFN and installed in the ALICE experiment at CERN-LHC have motivated a dedicated INFN project to perfection those detectors for the use in the frames of low energy X-ray detection down to energies of the order of the order of the KeV [32]. With a process of incremental innovation those detectors, of noticeable dimensions (about 7 x 7 cm^2), are at present developed in the direction of efficient, high resolution, reliable X-ray detection for advanced light sources. Silicon Drift Detectors in particular, because of their operation principle [33], are apt for the needed specific evolutionary processes.

Useless to say that such a high brightness linac might drive several other applications. For example the 700 MeV injector could be used, in a stand alone operational mode, to drive a Compton γ−ray source, as the one under study for the ELI_NP collaboration [21]. In this way γ−rays with energies of 10-20 MeV can be produced and directed head-on against electrons of 700 MeV. A reach physics program can be studied [30], which includes –among others- the precise measurement of the π^0 width through the process $e^- \gamma \rightarrow \pi^0 e^-$ (*Primakov effect*), and the search for light dark bosons in the energy region below 250 MeV [31]. These measurements, which provide important tests of the Standard Model, are not possible at present electron-photon colliders due to the low photon intensities of the machines.

Powerful THz radiation sources can be also considered. The accepted paradigm of condensed matter physics n fact is that the high-energy short-time dynamics affects the low-energy long-living degrees of freedom. Actually, pushing a system out-of-equilibrium, this hierarchy could be reversed. This determines a non-linear coupling among several degrees of freedom providing the possibility to coherently manipulate different states of matter. In this scenario, one can cite for instance the possibility to coherent induce a conformation transition in macromolecules, selectively pumping a low-energy collective mode; or even inducing a coherent structural phase transition through a phonon pumping. This "low-energy" manipulation can be obtained through strong terahertz (THz) sub-ps pulses associated to electric field in the order of 1 MV/cm. Broad band THz pulses showing these characteristics can be produced in a linac by using Transition Radiation (CTR) targets [23] or dipole radiation [22]. Single color THz radiation, can be also produced

combining a comb-beam with a CTR target [23]. A different scheme consists in a THz ondulator which could be mount at the end of the FEL ondulators. In this case the monocromatic THz radiation could be coupled to x-ray light for THz-pump x-ray diffraction probe experiments.

Last but not least, advanced accelerators concepts could be also tested, like Plasma acceleration or Dielectric wake field acceleration [24], to increase the final beam energy.

REFERENCES

[1] W.A. Barletta et al., "Free electron lasers: present status and future challenges", NIM-A 618 (2010).
[2] "SuperB Progress Report" http://arxiv.org/abs/1009.6178v3 .
[3] M. Xie, "Design Optimization For An X-Ray Free Electron Laser Driven By Slac Linac" , Proceedings PAC 1995, 183 (1996).
[4] M. Ferrario et al., "HOMDYN study for the LCLS RF photo-injector", SLAC-PUB-8400, (2000).
[5] S. Reiche,Nucl. Instr. and Meth. A 429 243 (1999).
[6] L. Giannessi et al., Self-amplified spontaneous emission for a single pass free-electron laser , Phys. Rev. ST Accel. Beams 14, 060712 (2011).
[7] L. Giannessi et al., Self-Amplified Spontaneous Emission Free-Electron Laser with an Energy-Chirped Electron Beam and Undulator Tapering, Phys. Rev. Lett. 106, 144801 (2011).
[8] M. Labat et al., High-Gain Harmonic-Generation Free-Electron Laser Seeded by Harmonics Generated in Gas , Phys. Rev. Lett. 107, 224801 (2011).
[9]L. Giannessi et al., High-Order-Harmonic Generation and Superradiance in a Seeded Free-Electron Laser,., Phys. Rev. Lett. 108, 164801 (2012).
[10] M. Quattromini , Magnetic Measurement System For The SPARC Insertion Devices, Proceedings of the 2008 EPAC Conference (2008).
[11] R. Bonifacio, C. Pellegrini, L. Narducci, Opt. Commun. 50, 313, (1984).
[12] R. Bonifacio et al., Phys. Rev. Let., 73, 1, (1994).
[13] M.Ferrario, V.Fusco, M.Migliorati, L. Palumbo, Int. Journal of Modern Physics A, Vol 22, No. 3 (2007) 4214-4234**.**
[14] L. Serafini, M. Ferrario, AIP Conf. Proc. 581 (2001) 87.
[15] M. Ferrario et al., Experimental Demonstration of Emittance Compensation with Velocity Bunching, Phys. Rev. Lett. 104, 054801 (2010).
[16] D. Alesini, M. Ferrario, V. Lollo, R. Di Raddo, V. Spizzo, L. Palumbo: "Design, Realization and Low Power RF Tests of the C Band Structure Prototype for SPARC", SPARC RF-11/002, 01/02/11.
[17] B. Spataro et al." High power comparison among brazed, clamped and electroformed X-band cavities", NIM-A-657 (2011) 88-93.
[18] L.M. Young (documentation by J.H. Billen). "PARMELA", report LA-UR-96-1835, Los Alamos,1996 (rev. 2004).
[19] M. Borland, "ELEGANT: A Flexible SDDS-Compliant Code for Accelerator Simulation" , Advanced Photon Source LS-287, September 2000.
[20] M. Ferrario et al., Beam dynamics in a high brightness linac for short wavelength SASE-FEL experiments, New J. Phys. 8 No 11 (November 2006) 295.
[21] http://www.e-gammas.com/

[22] http://www.sparx-fel.it/
[23] E. Chiadroni et al., “The THz radiation source at SPARC”, Journal of Physics: Conference Series 357 (2012) 012034.
[24] https://slacportal.slac.stanford.edu/sites/ard_public/facet/Pages/default.aspx
[25] M. Ferrario and T. Shintake, “High Performance Electron Injectors”’ Reviews of Accelerator Science and Technology, Vol. 3 (2010) 221–235.
[26] B. E. Carlsten, Nucl. Instrum. Methods A **285**, 313 (1989).
[27] L. Serafini, J. B. Rosenzweig, Phys. Rev. E **55** (1997) 7565.
[28] M. Ferrario et al., Phys. Rev. Lett. **99**, 234801 (2007).
[29] G. Geloni et al., “Production of transform-limited X-ray pulses through self-seeding at the European X-ray FEL”, DESY 11-165, September 2011.
[30] G. Venanzoni “Physics possibilities at a low energy e-γ collider” presentation at LIFE Meeting, Frascati March 16 2011
[31] M. Reece and L.-T. Wang,``Searching for the light dark gauge boson in GeV-scale experiments," JHEP {\bf 0907} (2009) 05.
[32] “Room-temperature spectroscopic performance of a very-large area silicon drift detector” (2011) Nuclear Instruments and Methods in Physics Research, Section A: Accelerators, Spectrometers, Detectors and Associated Equipment, 633 (1), pp. 15-21.
[33] The X-ray spectroscopic performance of a very large area silicon drift detector (2009) IEEE Transactions on Nuclear Science, 56 (3), art. no. 5075988, pp. 832-835.